Frequency locking and devil's staircase for a two-dimensional ferrofluid droplet in an elliptically polarized rotating magnetic field

S. Lācis,[1] J. C. Bacri,[2] A. Cēbers,[1] and R. Perzynski[2]
[1]*Latvian Academy of Sciences, Institute of Physics, Salaspils-1, LV-2169, Latvia*
[2]*Laboratoire d'Acoustique et Optique de la Matière Condensée**,
Université Pierre et Marie Curie, Tour 13, *Case* 78, 4 *place Jussieu*, 75252 *Paris Cedex* 05, *France*
(Received 28 February 1996; revised manuscript received 19 July 1996)

Numerical studies reveal that the dynamics of a magnetic fluid droplet under the action of an elliptically polarized rotating magnetic field can be quite complicated, including a transition to a chaotic behavior. On the basis of equations of motion derived by a virial method, the devil's staircase, and its Farey tree structure, is found for the time-averaged angular velocity of the droplet as a function of the angular velocity of the elliptically polarized field. By considering frequency locking (Arnold tongues) with respect to the magnetic Bond number, we establish multiple basins of attraction in different regions of the parameter space. The fractal character of basins of attraction is revealed and phenomena of hysteresis are shown from numerical scanning of the region of control parameters. The existence of period doublings and the transition to chaotic behavior at large field ellipticity parameters is suggested on the basis of phase space plots. [S1063-651X(97)00502-3]

PACS number(s): 47.52.+j, 75.50.Mm, 83.50.Lh

I. INTRODUCTION

A system with a nonzero magnetic dipole moment in a rotating magnetic field tends to follow the field rotation until some critical frequency is reached, at which time the friction torque can no longer be balanced by the magnetic torque [1]. At this point a ''breakoff'' takes place and the rotation of the dipole becomes ''jerky.'' In the case of an elliptically polarized field similar phenomena are observed for a bound pair of nonmagnetic particles in a magnetic fluid [2,3]. Interaction between magnetic and viscous forces leads to various modes of motion, classified as (1) steady-state rotation; (2) rotation with stops and backward motion; and (3) localized oscillations. Transitions between these modes are well described by a single nonlinear equation and depend on the frequency, the amplitude of the rotating field, the fluid viscosity, and the magnetic susceptibility. It is established, both experimentally and numerically [3] that for a pair of free spheres frequency locking takes place in an elliptical polarized field for $\Omega/\Omega_H=1/2$, 1/4, etc., where Ω is the average angular frequency of the pair rotation, and Ω_H is the angular frequency of the magnetic field rotation. Recent studies of a pair of rigid (undeformable) ferrofluid drops in a rotating magnetic field [4] display the existence of a frequency plateau in the high-frequency range for the pair rotation, thus demonstrating the relevance of internal rotations. Chaotic motion of a compass [5], and that of a permanent magnet rotor [6] in an oscillating field, are other well known examples of complex dynamic behavior in an oscillating field when the inertia of the system plays a considerable role. The behavior of a liquid microdroplet, typically 10 μm sized and made of a magnetic fluid (MF), has been experimentally studied under the action of a rotating magnetic field. It includes a wide variety of very complex phenomena in the high-frequency range [7]. In the low-frequency range the shape of such a droplet is close to a general ellipsoid [7,8]. This behavior, even at low frequencies, could be rather complex, since a droplet has more degrees of freedom than a rigid magnetic dipole under the action of a rotating field. For such a system the viscous energy dissipation is significant and the inertia plays no role due to the small size of droplets.

The response of a MF microdrop to a rotating magnetic field is studied numerically in two dimensions (2D) by the boundary element method (BEM) in [9]. In the low-frequency range the elongated droplet rotates with the frequency of a magnetic field. An increase in the field frequency may cause the motion of the droplet to go through a transition from a state in which the droplet follows the magnetic field with a constant phase lag, to a state in which the phase lag increases in a series of kinks. The transition takes place at a critical field frequency, which is a function of the field amplitude. Equations of the droplet motion are derived analytically and show good agreement with the BEM.

Two different types of steady-state behavior are observed depending on the magnetic field strength H. Both types of behavior are discerned by a critical value of the magnetic bond number

$$\mathrm{Bm}_{\mathrm{cr}}=\frac{H_{\mathrm{CR}}^2 R}{\sigma}=6\pi(\mu+1)^3/(\mu-1)^3, \qquad (1)$$

for a droplet of radius R, surface tension σ, and permeability μ. The bond number gives the threshold value for instability of a 2D MF circular droplet in a high-frequency rotating field with respect to the elliptical deformations [7,8,10]. At $\mu=15$ $\mathrm{Bm}_{\mathrm{cr}}=28.14$.

(i) ''Low-field'' behavior: If the magnetic bond number is less than the critical value, the droplet extension in stationary configurations diminishes as the rotating field frequency increases. The maximal phase lag value $\pi/4$ is reached at an infinite frequency.

*Associated with the Centre National de la Recherche Scientifique.

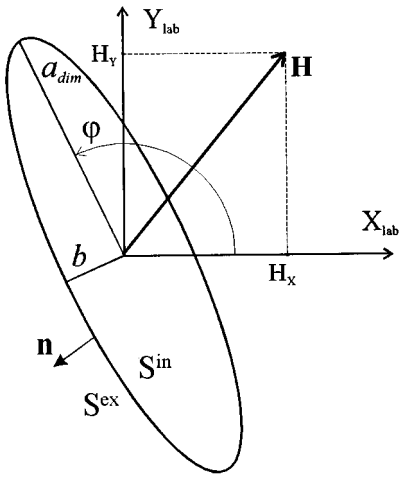

FIG. 1. Sketch of the droplet in laboratory coordinates.

(ii) ''High-field'' behavior: For magnetic bond numbers larger than the critical value the maximal phase lag ($\approx\pi/4$) is reached already at a finite critical frequency $\Omega_{\rm cr}$(Bm). It was shown in [9], by a linear analysis of small perturbations of differential equations, that for a motion near the stationary point, a finite viscosity inside the droplet brings about stabilizing effects and assists the droplet to follow the magnetic field rotation. At ''high-field'' values it results in time-averaged frequency jumps from the field frequency Ω_H to some smaller value just above the critical frequency $\Omega_{\rm cr}$. By increasing the ratio of viscosities $\lambda=\eta_{\rm in}/\eta_{\rm ex}$ the critical frequency $\Omega_{\rm cr}$ may be slightly reduced to approach the analytical value $\Omega_{\rm cr0}$ [see relation (14) further in the text].

Preliminary simulations have shown [9] that in the case of rotating elliptically polarized magnetic fields the frequency locking takes place as demonstrated in [3]. Frequency locking and observation of the devil's staircase in a phase plane Ω/Ω_H versus Ω_H is the subject of the present paper.

II. EQUATIONS OF MOTION FOR A 2D ELLIPTIC DROPLET IN AN ELLIPTICAL ROTATING FIELD

We made use of the equations of motion derived in [9] and improved in [11]. The set of equations describes a MF droplet in a low-frequency rotating field under the assumption of a 2D elliptic shape and accounts for shear flow occurring inside the droplet. A 2D Stokes flow problem outside the droplet is solved exactly, whereas the flow inside is described in the approximation of constant velocity gradients. Dynamic boundary conditions are satisfied integrally by employing the virial moment technique. Arbitrary viscosities of a fluid inside and outside the droplet are considered. The small size of a microdroplet and relatively small characteristic velocities of a flow allow us to neglect inertia and gravity terms, thus focusing attention on surface tension and magnetic forces on the surface of the droplet. Hence, the dynamics of the free surface of the droplet can be described within a framework of the creeping flow model.

An elliptic incompressible MF droplet is completely determined by the length of its large semiaxis $a_{\rm dim}$ and the angle φ of its orientation with respect to the $X_{\rm lab}$ axis of the laboratory frame (see Fig. 1). To conserve the elliptic shape of the droplet the flow inside the droplet is approximated by constant gradients γ_{ik} of velocity field

$$\nu_i=\gamma_{ik}x_k. \tag{2}$$

Consequently, equations of motion [11] may be expressed in a nondimensional form in the following way:

$$\dot a=\frac{2a^4}{\pi(a^4+1+2\lambda a^2)}\left[\frac{(\mu-1)^2}{16}\,{\rm Bm}a\left(\frac{H_{0a}^2}{H_0^2}\,\frac{1}{(a^2+\mu)^2}-\frac{H_{0b}^2}{H_0^2}\,\frac{1}{(a^2\mu+1)^2}\right)-\frac{\Phi(a)}{a^4-1}\right], \tag{3}$$

$$\dot\varphi=\frac{H_{0a}H_{0b}}{H_0^2}\,\frac{\rm Bm}{8\pi}\,\frac{(\mu-1)^2a^2}{(a^2+\mu)(a^2\mu+1)}\times\frac{2a^2\,\dfrac{a^4+1}{a^4-1}+\lambda(a^4-1)}{2a^2+\lambda(a^4+1)}. \tag{4}$$

Here H_{0a} and H_{0b} are the instantaneous projections of the external field intensity on both axes of an elliptical droplet,

$$\Phi(a)=[(a^4+1)E(e)-2K(e)],$$

$$\lambda=\eta_{\rm in}/\eta_{\rm ex},\quad a=a_{\rm dim}/R,$$

where

$$E(e)=\int_0^{\pi/2}\sqrt{1-(e\,\sin x)^2}\,dx$$

and

$$K(e)=\int_0^{\pi/2}1/\sqrt{1-(e\,\sin x)^2}\,dx$$

are complete elliptic integrals of the first, respectively, second kind, $e^2=1-b^2/a^2$, $\eta_{\rm in}$, $\eta_{\rm ex}$: viscosities of fluid inside, respectively, outside the droplet.

The radius of a circular drop $R=\sqrt{a_{\rm dim}b_{\rm dim}}$ and a time scaling unit $\tau_b=R\,\eta_{\rm ex}/\sigma$ are used to obtain a nondimensional form of equations. The interplay of magnetic forces and surface tension is characterized by the magnetic bond number ${\rm Bm}=H_0^2R/\sigma$.

The main improvement in comparison with the equations considered in [9] is a more adequate representation of the extensional motion of a droplet as well as of the rotational motion caused by the shear flow inside a droplet. Comparison with results of numerical simulations by BEM proves that these equations of motion can be used to simulate the behavior of a droplet in a magnetic field with a fairly good accuracy.

In the case of an elliptic field polarization, instantaneous components of the external magnetic field are given by the following relations:

$$H_X(t)=H_{0X}\cos(\Omega_Ht),$$

$$H_Y(t)=H_{0Y}\sin(\Omega_Ht). \tag{5}$$

By assuming $H_{0X} \geqslant H_{0Y}$ the parameter γ is introduced to control the magnetic field ellipticity

$$H_{0X} = H_0\sqrt{1+\gamma}, \tag{6}$$

$$H_{0Y} = H_0\sqrt{1-\gamma},$$

$$\gamma = \frac{H_{0X}^2 - H_{0Y}^2}{H_{0X}^2 + H_{0Y}^2}. \tag{7}$$

The above provision allows us to keep the effective magnetic bond number $\mathrm{Bm} = H_0^2 R/\sigma$ constant by fixing the mean square value of the external field which in turn is achieved by selecting H_0 for any γ value

$$\overline{H^2} = \overline{[H_{0X}\cos(\Omega_H t)]^2 + [H_{0Y}\sin(\Omega_H t)]^2}$$
$$= \tfrac{1}{2}(H_{0X}^2 + H_{0Y}^2) = H_0^2. \tag{8}$$

Hence, the elliptically polarized field is defined by its ''average'' intensity H_0 and the ellipticity parameter γ. For a physical interpretation, the elliptically polarized field can be divided in a pure rotational field $\mathbf{H}_{\mathrm{rot}}$ with the following components:

$$H_{X,\mathrm{rot}}(t) = H_0\sqrt{1-\gamma}\,\cos(\Omega_H t),$$

$$H_{Y,\mathrm{rot}}(t) = H_0\sqrt{1-\gamma}\,\sin(\Omega_H t),$$

and a nondimensional amplitude $h_{\mathrm{rot}} = \sqrt{1-\gamma}$, and a pure linearly oscillating field $\mathbf{H}_{\mathrm{osc}}$ with components

$$H_{X,\mathrm{osc}}(t) = H_0(\sqrt{1+\gamma} - \sqrt{1-\gamma})\cos(\Omega_H t),$$

$$H_{Y,\mathrm{osc}}(t) = 0,$$

and a nondimensional amplitude $h_{\mathrm{osc}} = \sqrt{1+\gamma} - \sqrt{1-\gamma}$. By increasing γ from 0 to 1 the rotational field amplitude h_{rot} tends to approach 0, whereas the oscillating field amplitude h_{osc} increases from 0 to $\sqrt{2}$.

The instantaneous projections H_{0a}, H_{0b} of the external field intensity in the directions of both axes of an elliptic droplet are implemented in Eqs. (3) and (4), and derived as

$$H_{0a}(t) = H_X(t)\cos\varphi + H_Y(t)\sin\varphi,$$

$$H_{0b}(t) = -H_X(t)\sin\varphi + H_Y(t)\cos\varphi. \tag{9}$$

Let us introduce the two nondimensional components of the field in the direction of the semiaxes of an elliptic droplet $h_a = H_{0a}/H_0$ and $h_b = H_{0b}/H_0$. Then

$$h_a^2 = [1 + \cos2\varphi_H\cos2\varphi + \gamma(\cos2\varphi_H + \cos2\varphi)$$
$$+ \sqrt{1-\gamma^2}\sin2\varphi_H\sin2\varphi]/2, \tag{10}$$

$$h_b^2 = [1 - \cos2\varphi_H\cos2\varphi + \gamma(\cos2\varphi_H - \cos2\varphi)$$
$$- \sqrt{1-\gamma^2}\sin2\varphi_H\sin2\varphi]/2, \tag{11}$$

$$h_a h_b = [-\cos2\varphi_H\sin2\varphi - \gamma\sin2\varphi$$
$$+ \sqrt{1-\gamma^2}\sin2\varphi_H\cos2\varphi]/2. \tag{12}$$

Here $\varphi_H = \Omega_H t$. In the case of a circular field polarization ($\gamma = 0$) we have

$$h_a^2|_{\gamma=0} = \cos^2(\varphi_H - \varphi),$$

$$h_b^2|_{\gamma=0} = \sin^2(\varphi_H - \varphi),$$

$$h_a h_b|_{\gamma=0} = \sin2(\varphi_H - \varphi)/2.$$

It follows from the above relations that in the case of a circular field polarization, the rigid droplet limit ($\lambda \to \infty$) is analogous to a bound pair of soft magnetic particles [2]

$$\dot{\varphi} = \Omega_{\mathrm{cr}}\sin2(\varphi_H - \varphi), \tag{13}$$

$$\Omega_{\mathrm{cr}} = \frac{\mathrm{Bm}}{16\pi}\,\frac{(\mu-1)^2 a^2(a^4-1)}{(a^2+\mu)(a^2\mu+1)(a^4+1)}. \tag{14}$$

The time-averaged frequency $\overline{\Omega}$ of a droplet rotation is defined as

$$\overline{\Omega} = \lim_{T\to\infty}\frac{1}{T}\int_0^T \dot{\varphi}\,dt. \tag{15}$$

An analytical integration for Eq. (13) gives the following expression for $\overline{\Omega}$:

$$\overline{\Omega} = \Omega_H - \sqrt{\Omega_H^2 - \Omega_{\mathrm{cr}}^2}. \tag{16}$$

It is worth noting that the value of a is fixed: it corresponds either to a ''rigid droplet'' approximation ($\lambda \gg 1$) or a ''high-frequency'' approximation ($\Omega_H \gg \Omega_{\mathrm{cr}}$). Provided $\Omega_H/\Omega_{\mathrm{cr}} \to \infty$, the approximation of ''very high'' frequencies is reached yielding

$$\overline{\Omega} \approx \frac{\Omega_{\mathrm{cr}}^2}{2\Omega_H}. \tag{17}$$

It is reported in [4] that after a jerky regime, the frequency of a pair rotation reaches a plateau independent of Ω_H. Hence, at sufficiently high frequencies ($\Omega_H/\Omega_{\mathrm{cr}} \gg 10$) the above approximations could be too rough to describe the behavior of a droplet. Therefore it might be necessary to account for effects like internal rotation.

The elongation of a droplet depends on the intensity of an applied magnetic field. In the stationary case $\dot{a} = 0$ and the major semiaxis a could be obtained from Eq. (4)

$$\frac{(\mu-1)^2}{32}\,\mathrm{Bm}a\left(\frac{1}{(a^2+\mu)^2} - \frac{1}{(a^2\mu+1)^2}\right) = \frac{\Phi(a)}{a^4-1}. \tag{18}$$

The dependence of a on Bm is plotted in Fig. 2. Curves for different μ values certify that the influence of the magnetic permeability on the droplet extension could be very strong. Above the magnetic field threshold an instability with respect to elliptic shape perturbations may occur. Depending on the magnetic permeability, it is instability either of the first kind ($\mu < 10.71$) or of the second kind ($\mu > 10.71$) [10]. In the case of an elliptic field polarization the equation for phase lag (4) in the rigid droplet limit $\lambda \to \infty$ becomes

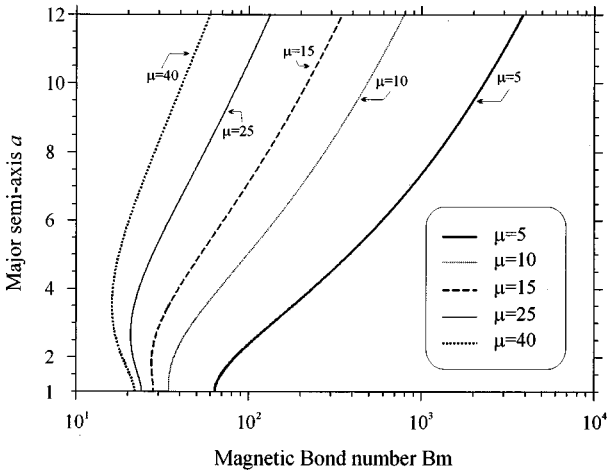

FIG. 2. Droplet extension in a time-averaged high-frequency rotating magnetic field.

$$\dot{\varphi}=\Omega_{\rm cr}[-\cos 2\varphi_H \sin 2\varphi-\gamma\sin 2\varphi + \sqrt{1-\gamma^2}\sin 2\varphi_H\cos 2\varphi]. \tag{19}$$

To obtain $\overline{\Omega}$ analytical integration of Eq. (19) is obviously not feasible.

III. NUMERICAL TECHNIQUE AND FREQUENCY LOCKING IN AN ELLIPTICALLY POLARIZED FIELD

To solve the system of equations of motion (3) and (4), the fourth-order Runge-Kutta algorithm is applied. The time-averaged frequency Ω is obtained in the following way: at first in order to achieve attractor from the basin chosen by initial conditions a numerical algorithm is run during a specified transition time T_t. After N field revolutions the winding number [12]

$$w_N=\frac{1}{2\pi N}\int_{T_t}^{T_t+2\pi N/\Omega_H}\dot{\varphi}dt=\frac{\varphi_H-\varphi_0}{2\pi N} \tag{20}$$

is found. The averaged frequency $\overline{\Omega}=w_N\Omega_H$ could be found with an arbitrary accuracy by increasing N. Truncation errors, as well as the accuracy of the Runge-Kutta algorithm, should be taken into account. In Fig. 3(a) the winding number $w_N=\overline{\Omega}/\Omega_H$ is plotted versus the field frequency Ω_H, Bm=50, μ=15, λ=5, γ=0.15. The time step employed in the different calculations below equals Δt=0.01. The solid curve depicts the winding number w obtained by increasing the field frequency, the dashed one by decreasing it. Two new phenomena are introduced by the elliptic field polarization: frequency locking in certain frequency ranges and overlapping of modes. The first two frequency-locking intervals $w_{1/1}$ and $w_{1/2}$ are rather wide and correspond to the frequency range in which the droplet rotation is stabilized in the case of the circular field because of the finite value of λ. The overlapping of the modes results in a hysteresis: increase in the field frequency causes a jump in the phase plane from the mode $w_{1/1}$ directly to the mode $w_{1/2}$ passing over nonexistent modes of winding numbers between 1 and 0.5. A decrease in the field frequency attests that the mode $w_{1/2}$ overlaps with the mode $w_{1/1}$ prior to a jump back to the mode $w_{1/1}$. A further increase in the field frequency causes principal sequential frequency lockings $w_{1/3}$, $w_{1/4}$, $w_{1/5}$ to take place, i.e., the principal sequence of the frequency locking exhibits itself. According to the Farey tree law between two modes with winding numbers p_1/q_1 and p_2/q_2 there shall be another mode $(p_1+p_2)/(q_1+q_2)$. Hereafter $w_{p/q}=\overline{\Omega}/\Omega_H=p/q$, where p,q are integer, is used to denote frequency ratios. The classical devil's staircase [12,13] has a fractal

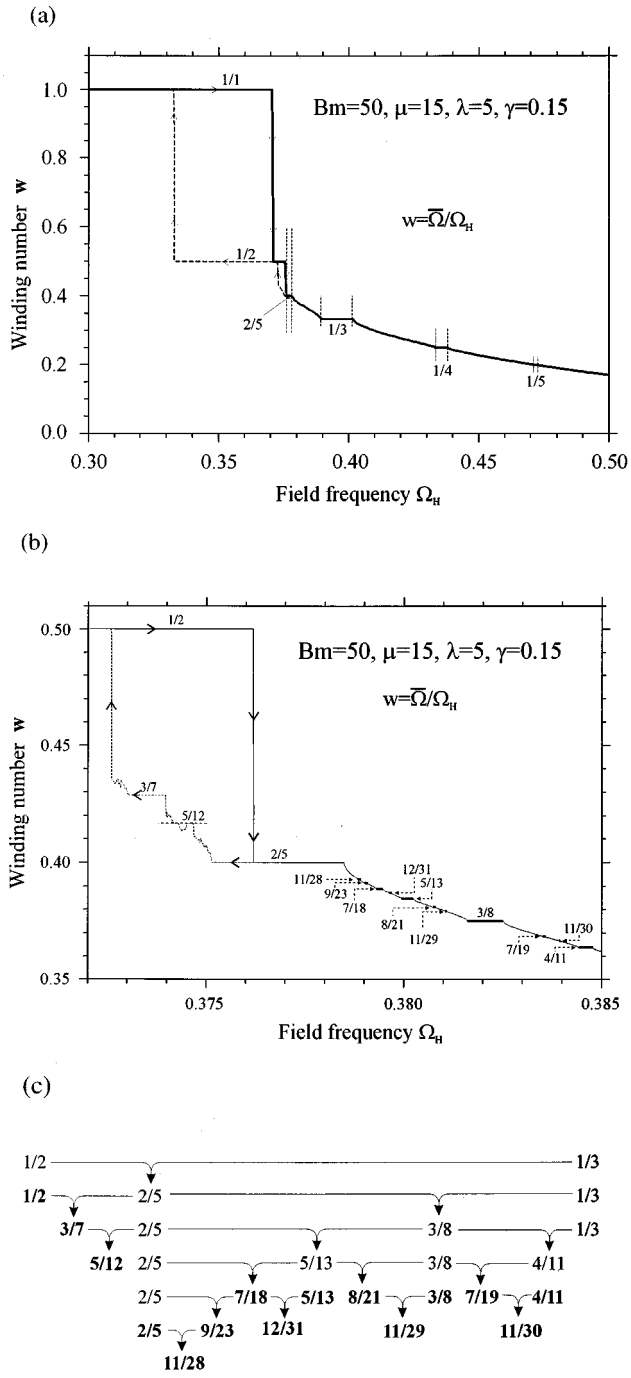

FIG. 3. (a),(b) (expanded view). Winding number w vs magnetic field frequency Ω_H. Bm=50, μ=15, λ=5. Field ellipticity parameter γ=0.15. The solid line corresponds to the increase of frequency and the dashed one to its decrease. (c) Farey tree construction of the observed frequency-locking intervals.

structure where sequentially all the ratios from the Farey tree [12] are present. Here one may see a degenerated devil's staircase since an overlapping takes place and winding numbers between modes $w_{1/1}$ and $w_{1/2}$ are not present. Obviously degeneration could be eliminated by increasing λ, since it diminishes the stability of the droplet rotation with the field frequency (see Fig. 10).

Another overlapping of frequency-locking intervals takes place at field frequencies in the range of about $0.372 \leqslant \Omega_H \leqslant 0.376$ where the mode $w_{1/2}$ is detected at the increase of the frequency [see Figs. 3(a), 3(b)]. A frequency decrease displays a few smaller frequency-locking steps ($w_{2/5}$, $w_{5/12}$, and $w_{3/7}$) and rather complex behavior between the steps. In accordance with properties of the devil's staircase the intervals of complex behavior could consist of frequency-locking intervals. However, their width may be too small to be detected using the frequency step $\Delta\Omega_H = 0.0005$ employed for present calculations.

In Fig. 3(b) the frequency range $0.372 \leqslant \Omega_H \leqslant 0.385$ is magnified for the sake of comparison with Fig. 3(a). The left part of the plot is degenerated due to the overlapping of modes already mentioned above. For frequencies larger than $\Omega_H = 0.377$ the character of the curve changes into the classical devil's staircase [13], the winding numbers for frequency-locking intervals correspond closely to the Farey tree [12,13] as shown in Fig. 3(c). At magnification one can see quite well the self-similarity of the devil's staircase in the specified frequency range.

It is evident from Eqs. (3) and (4) that the motion depends on five parameters: Bm, μ, λ, γ, Ω_H. Here we do not intend to discuss the influence of the magnetic permeability μ on solutions, however it should be pointed out that μ cannot be simply eliminated from the equations of motion by including it inside the magnetic bond number since there are two terms like $(a^2+\mu)$ and $(a^2\mu+1)$ which contain both a and μ. In the present paper we focus on the case of $\mu = 15$ which corresponds to an intermediate value of μ, since special effects, caused by different choices of μ have not yet been detected.

IV. FREQUENCY LOCKING IN DEPENDENCE ON MAGNETIC BOND NUMBER

The behavior of a MF droplet in a circular rotating magnetic field has already been described above. It presents two different scenarios [9] corresponding to ''low-field'' or ''high-field'' regimes.

Similar properties are inherited in the case of the elliptic field polarization. In Fig. 4 frequency-locking domains are plotted in the phase plane Bm versus Ω_H. One can clearly see the field threshold, below which only one mode $w = w_{1/1}$ (the droplet locked to the field) corresponding to scenario I may exist. Above this threshold different frequency-locking domains may appear. An increase of Bm results in practically no changes regarding the width or the slope of domain boundaries.

The principal sequence of the frequency locking may be arrived at $w_{1/q}$, where q is an integer. As a general rule, all the subsequent locks become more and more narrow and hence harder to detect. If the width of the frequency-locking plateau becomes smaller than the frequency step of the numerical algorithm, one fails to observe any frequency locking. Behavior of frequency locking seems to be more or less regular from the frequency range of the mode $w_{1/3}$ to infinity as well as for Bm larger than 40; i.e., the boundaries of the frequency-locking domain are parallel with a fixed slope. By increasing q, the frequency width of the frequency locking $w_{1/q}$ decreases. A rather broad overlapping of domains for the modes $w_{1/1}$ and $w_{1/2}$ takes place for lower frequencies. On the contrary, there is no overlapping between the modes $w_{1/2}$ and $w_{2/5}$.

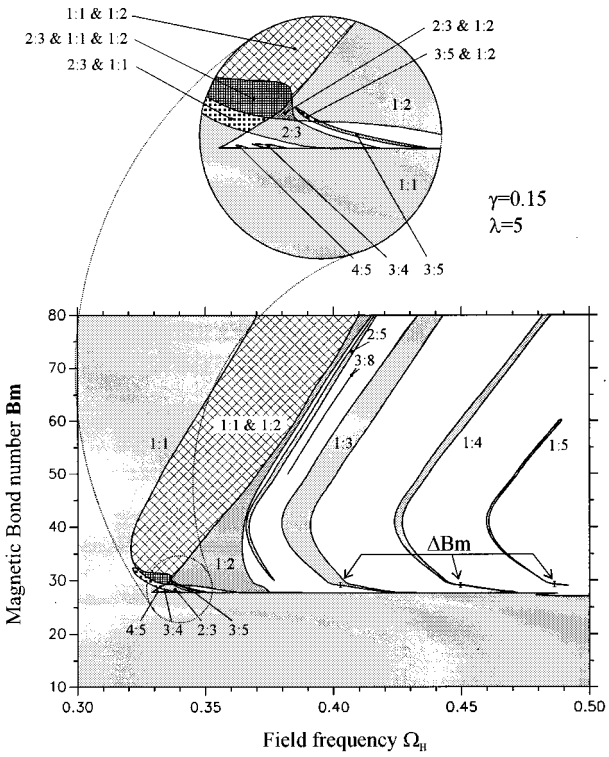

FIG. 4. Frequency-locking domains (Arnold tongues) in the phase plane Bm vs Ω_H. $\gamma = 0.15$, $\mu = 15$, $\lambda = 5$. Near the origin of Arnold tongues scanning step ΔBm is shown by error bars. A scanning step along the Ω_H axis is smaller than 0.0002. At larger values of Bm a scanning step may be taken larger because boundaries of Arnold tongues are nearly straight lines at that range.

A more complex behavior is observed for $28 < \mathrm{Bm} < 34$ and field frequencies $0.32 < \Omega_H < 0.36$. An expanded view of this section of the phase space is reflected in Fig. 4. Boundaries for frequency-locking domains $w_{4/5}$ and $w_{3/4}$ may not be determined exhaustively due to the finite numerical methods, whereas the domain boundaries for locking of winding numbers $w_{1/1}$, $w_{1/2}$, $w_{2/3}$, and $w_{3/5}$ are detected more accurately. These values are presented in more detail in a magnified plot, where overlapping of four modes takes place in the point ($\Omega_H = 0.335$, $\mathrm{Bm} = 30.5$) of the parameter space. Trajectories of the droplet's tip in the laboratory coordinates are depicted in Fig. 5. The trajectories exhibit a rather stable motion without any transition. The selection of the mode in which a droplet locks itself depends on the initial conditions. To illustrate it, the basins of attraction [14] are plotted in Fig. 6. This map represents the laboratory coordinates of the droplet tip at an initial moment ($t = 0$) at which a magnetic field according to Eq. (5) has only a positive X component. The basin of attraction leading to the mode $w_{1/2}$ consists of

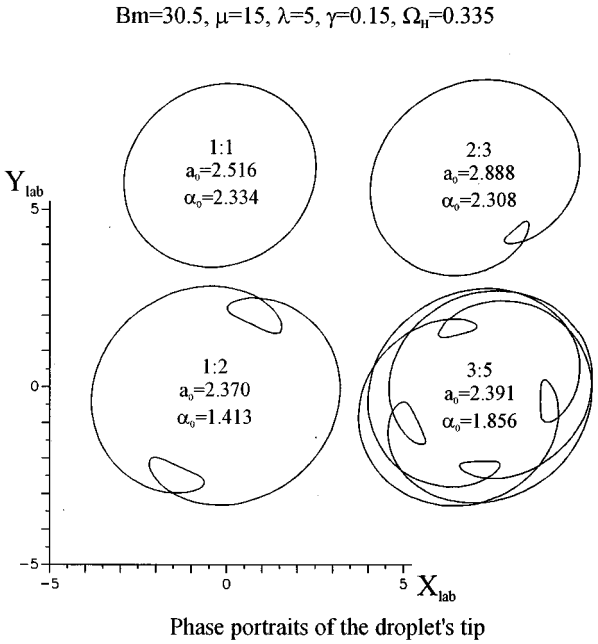

FIG. 5. Four different modes for the point ($\Omega_H=0.335$, Bm $=30.5$) of the phase plane. $\mu=15$, $\lambda=5$, $\gamma=0.15$.

four domains. These are separated by the mode $w_{3/5}$, as is displayed in the diagram. Domains of initial conditions for the mode $w_{1/1}$ are concentrated near the corresponding Poincaré sections at time moments $t_n=n\pi/\Omega_H$. The structure of the spiral tails of these domains is interesting: it, as well as initial points for mode $w_{2/3}$, exhibits fractal-like properties, illustrated by the expanded view of the present picture, shown in Fig. 7. In both diagrams the mode $w_{1/1}$ is shown by empty circles, $w_{1/2}$: by crosses, $w_{2/3}$: by filled circles, and

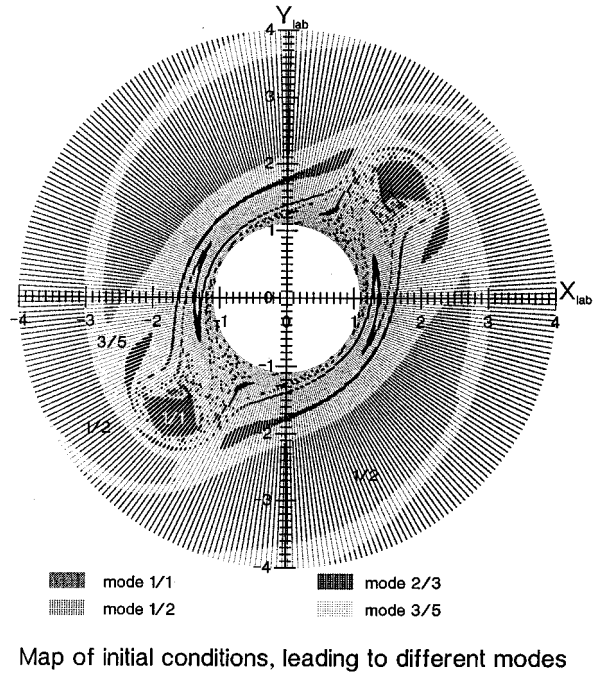

FIG. 6. Map of initial conditions for four different modes of Fig. 5. Mode $w_{1/1}$: empty circles, $w_{1/2}$: crosses, $w_{2/3}$: filled circles, $w_{3/5}$: ''-'' (hyphens).

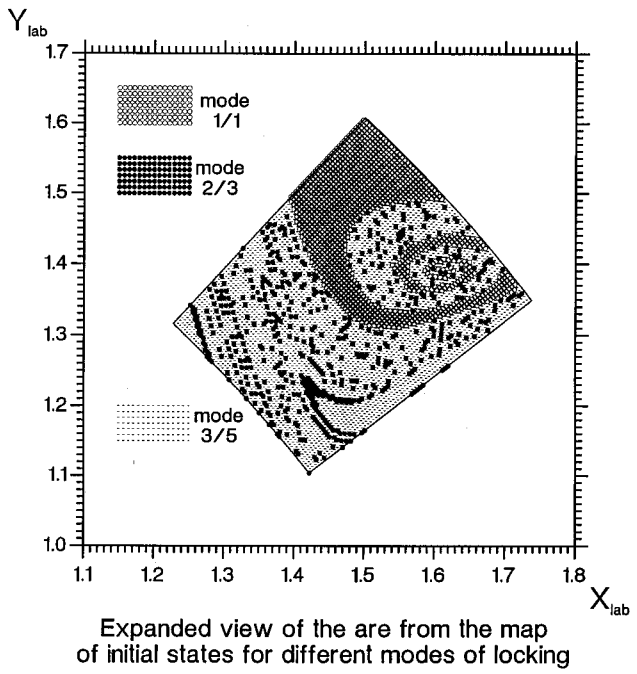

FIG. 7. Expanded view of the area from Fig. 6. Mode $w_{1/1}$: empty circles, $w_{1/2}$: crosses, $w_{2/3}$: filled circles, $w_{3/5}$: ''-'' (hyphens).

the mode $w_{3/5}$ by small ''-'' characters (hyphens). The main conclusion drawn from both figures indicates that the mode could be very sensitive to the choice of initial conditions of evolution.

V. DEPENDENCE OF FREQUENCY LOCKING ON THE FIELD ELLIPTICITY PARAMETER

Another important question pertains to the behavior of the threshold of the magnetic field at a fixed frequency and different values of the ellipticity parameter γ of the field polarization. Figure 8 shows that an increase in γ of up to $\gamma\approx0.3$ causes negligible change in the threshold value thus confirming that the field threshold value is characterized by the magnetic bond number. The two curves in Fig. 8 are indicative of an increasing bond number (solid curve) and a decreasing

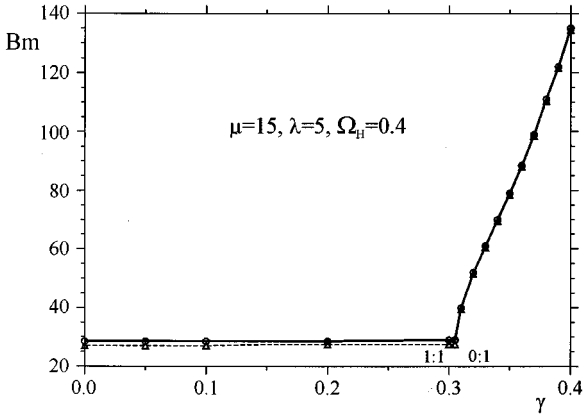

FIG. 8. Magnetic field threshold vs the ellipticity parameter γ of the field polarization.

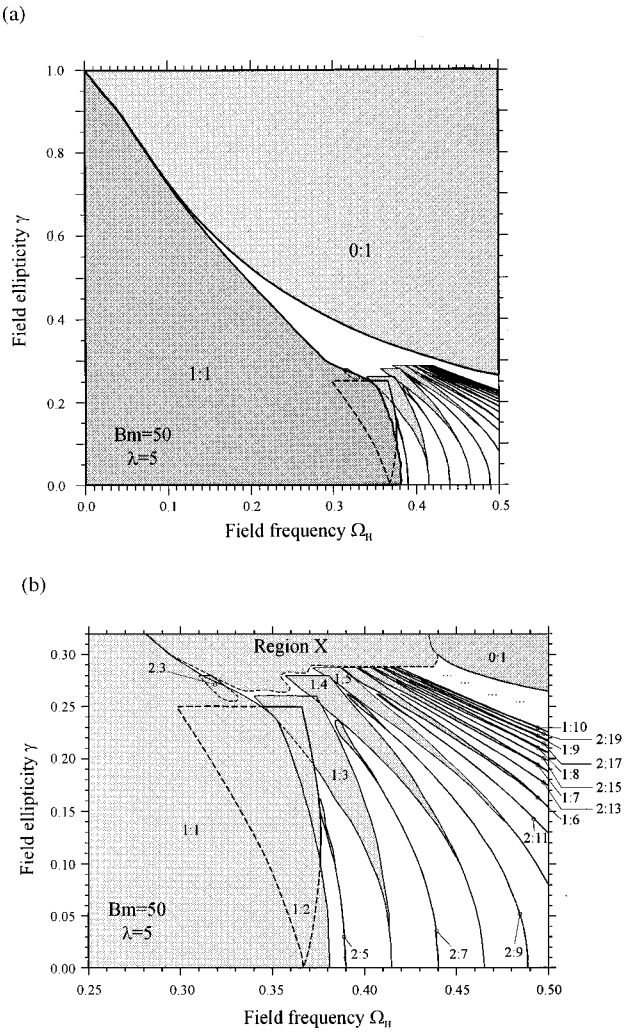

FIG. 9. Arnold's tongues diagram in the phase plane defined by the field ellipticity parameter γ and the field frequency Ω_H. (a) Frequency-locking domains for $w_{1/1}$ and $w_{0/1}$. (b) Expanded view of the frequency-locking domains for intermediate γ values.

bond number (dashed curve); the shift between these displaying the presence of a hysteresis which magnitude corresponds quite well to the magnitude of hysteresis for droplet elongation in a quasistatic field [10]. If γ reaches some limiting value, the droplet is locked by the oscillating component of the field and the rotating component is too weak to cause the rotation of the droplet, the tip of the droplet may only provide small localized oscillations (mode $w_{0/1}$).

Influence of γ on the frequency locking to $w_{0/1}$ is observed in Fig. 8, i.e., the mode of localized oscillations without rotation of a droplet may be observed. The critical γ value equals about $\gamma=0.3$–0.4 (Bm=30–140). This corresponds to the amplitude of a pure rotating field $h_{\rm rot}=0.84$–0.77, whereas the amplitude of a pure oscillating field equals $h_{\rm osc}=0.30$–0.55 undimensional units. The maximum γ value for the droplet rotation increases as the value of Bm is raised. Upon increasing Bm, the rise in the magnetic torque turns out to be more significant than the rise in the friction torque thus the droplet can perform full revolutions of up to a slightly higher γ limit (see Fig. 8)

Traditional representation of the frequency-locking phenomena depending on the control parameter is the so-called Arnold's tongue diagram [13,15]. Figure 9(a) plots frequency-locking domains in the phase plane of the field ellipticity parameter γ versus the field frequency Ω_H for Bm $=50$, $\mu=15$, $\lambda=5$. Two modes $w_{1/1}$ and $w_{0/1}$ predominate in the frequency range Ω_H without any overlapping. The space between these modes is filled with Arnold's tongues for other modes at $\gamma<0.275$. The boundaries of the domains $w_{1/1}$ and $w_{0/1}$ are quite smooth, except for a quite sharp decrease in the slope of the mode $w_{1/1}$ at γ of about 0.275. The value of $\gamma=0.275$ turns out to be near the critical γ value above which the droplet motion becomes chaotic and Arnold's tongues lose their orderly structure. Qualitative phase plots show that period doublings and transition to chaotic dynamics take place in the above region. The droplet behavior for $\gamma>0.275$ (Region X) illustrated by the phase space plots, Lyapunov indices, and Fourier spectra will be addressed in future publications. Expanded view of Fig. 9(a) below $\gamma=0.3$ is given in Fig. 9(b). Flat top boundaries of the tongues close to ''Region X'' are approximate; detailed investigation of the structure requires further studies. We would also like to point out that one can see two sequences of frequency locking in Fig. 9(b); the principal sequence is represented as $1/q$, the second one as $2/(2q+1)$, where q is the integer. Beyond $w_{1/10}$ the structure of tongues becomes too dense to be shown, intervals ''…'' are used to substitute $w_{1/q}$ and $w_{2/(2q+1)}$, for $q>10$. A unique property of the present system is the overlapping of modes $w_{1/1}$ and $w_{1/2}$: even at $\gamma\rightarrow 0$ a complete overlapping takes place. The placement of the frequency-locking domain $w_{2/3}$ at γ of about 0.27 and $\Omega_H\approx 0.35$ looks curious, but in fact it evidently may be explained with common properties of the structure of Arnold's tongues in the case of a supercritical regime [16]. Throughout all the present work, we use value $\gamma=0.15$ every time when parameter γ is fixed (i.e., when it is constant). This value of γ is regarded as a moderate value of the control parameter for the field ellipticity.

VI. DEPENDENCE OF FREQUENCY LOCKING ON THE VISCOSITY RATIO

An increase in λ corresponds to an increase of the viscosity ratio. Here we may discuss the case $\lambda=5$, a case of moderate MF viscosity compared to [7], where $\lambda\approx 100$. 2D simulations using the boundary element method [17] show that in the case of an arbitrary shape (without the constraint of an elliptic shape), a ferrofluid droplet displays a transition to an ''*S*''-like shape for $\lambda\gg 1$ and even for $\lambda=5$. Nevertheless, the results of present studies could be applied because for $\lambda=5$ the bending just slightly eliminates effective extension of the droplet and thus causes a minor decrease in the friction coefficient. General properties of droplet rotation still remain identical.

Arnold's tongues are plotted in the phase plane λ (log-scale) versus Ω_H in Fig. 10. The values of passive parameters are Bm=50, $\mu=15$, $\gamma=0.15$. The overlapping of modes $w_{1/1}$ and $w_{1/2}$ is a common phenomenon up to $\lambda=115$; for larger values of λ modes do not overlap. Overlapping of modes $w_{1/2}$ and $w_{1/3}$ occurs only at λ values of up to $\lambda\approx 1.5$. In general, an increase in λ thins down the frequency-locking width thus tending to eliminate the overlapping. Neverthe-

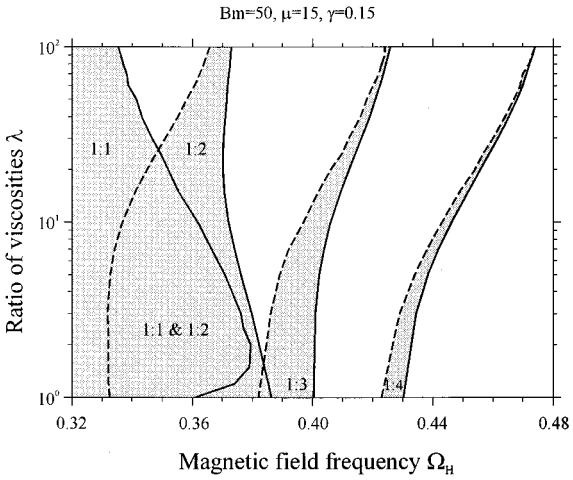

FIG. 10. The dependence of the width of frequency locking on the droplet viscosity, Arnold's tongues diagram in the phase plane defined by the ratio of viscosities λ, and the field frequency Ω_H.

less, at $\lambda=100$ the width of the mode $w_{1/2}$ is still quite commensurable with the distance from the mode $w_{1/2}$ to adjacent modes $w_{1/1}$ and $w_{1/3}$. The second property of λ is attributed to the shift of frequency-locking towards larger frequencies, with λ increasing.

The way the frequency-locking width depends on λ follows from general mechanisms of frequency locking for a ferrofluid droplet in an elliptically polarized magnetic field. In the present study the ellipticity of the field polarization, in fact, is the key parameter for the frequency-locking phenomena. Since inertia plays no role in the oscillations of droplet due to its small size, to have a frequency locking there have to be two oscillatory motions. One oscillation frequency quite naturally is maintained by the rotational component of a magnetic field $\mathbf{H}_{\rm rot}$. Another one is introduced into the motion of the droplet by a pure oscillatory field $\mathbf{H}_{\rm osc}$. A sketch of the mechanism of frequency locking in the present study follows. The $\mathbf{H}_{\rm rot}$ causes either a steady rotation of the droplet or a nonsteady one but periodic rotation with oscillations provided the field frequency exceeds the critical one [9]. In the last case, the frequency of droplet rotation is less than that of a field. Pure linear oscillations of a magnetic field causes droplet oscillations in X-axis direction at frequency of $2\Omega_H$. Amplitudes of both oscillations markedly depend on λ: increase in λ causes reduction of amplitudes. In the limit of $\lambda\to\infty$ (rigid droplet) the elongation of the droplet is fixed (constant) and only the phase lag between the magnetic field and the droplet could oscillate according to Eq. (19). Since for a system without inertia the self-resonance is absent, two ''external'' frequencies are required in order to realize the frequency locking. Hence, a rigid droplet, as well as a droplet in a pure circularly polarized magnetic field, fails to exhibit any frequency locking. Naturally, a ''soft'' droplet in the field-following regime has the simplest frequency locking of $w_{1/1}$. If the field frequency exceeds the critical one, a breakoff of the droplet takes place and it rotates at a lower frequency than the field frequency [see approximation (16)]. In that region other as $w_{1/1}$ frequency locked regimes take place.

VII. CONCLUSIONS AND DISCUSSION

It is shown that the angular velocity of a 2D ferrofluid droplet in an elliptically polarized field exhibits a frequency locking to the magnetic field rotation exhibiting a devil's staircase structure. Dependence of Arnold's tongues on the control parameters of the system are calculated. The coexistence of different frequency-locking regimes as shown by the hysteresis phenomena with variation of the control parameters is demonstrated by numerical calculations. The choice of a definite mode is very sensitive to initial conditions. The fractal character of the basins of attraction found numerically for different frequency-locked modes serves as an illustration. Beyond the critical value of the field ellipticity parameter the behavior of the droplet becomes chaotic as shown by phase space plots.

Although frequency locking in the present paper is established for a two-dimensional magnetic liquid droplet, there are good reasons to believe that this phenomenon also exists in three dimensions, since the physics inferred is essentially the same. It can possibly be observed as a staircaselike dependence for the torque, which acts on the container with a ferroemulsion, at the frequency of an elliptically polarized field.

Results of the present work can serve as a guideline for observation of the various frequency-locked modes in the case of a real three-dimensional magnetic droplet, which offers new experimental possibilities for studies of complex dynamics and transition to the chaos. Also within a frame of the present 2D magnetic fluid droplet model it is possible to overcome the usual problem of reducing the set of hydrodynamic equations to some finite dynamical system by studying the frequency locking and the transition to chaotic dynamics employing an exact boundary integral equation technique.

ACKNOWLEDGMENTS

This work was supported by ''Le Réseau Formation Recherche No. 90R0933 du Ministère de l'Enseignement Superieur et de la Recherche'' of France. Two of us (A.C. and S.L.) are grateful to International Science Foundation for financial support of research under a long-time Grant LJQ100. J.C.B. is affiliated with Université Paris 7.

[1] R. E. Rosensweig, *Ferrohydrodynamics* (Cambridge University Press, New York, 1985).

[2] G. Helgessen, P. Pieranski, and A. T. Skjeltorp, Phys. Rev. Lett. **64**, 1425 (1990).

[3] A. T. Skjeltorp and G. Helgessen, Physica A **176**, 37 (1991).

[4] J.-C. Bacri, C. Drame, B. Kashevsky, S. Neveu, R. Perzynski, and C. Redon, Prog. Colloid Sci. **98**, 124 (1995).

[5] V. Croquette and C. Poitou, J. Phys. Lett. **42**, L-527 (1981).

[6] F. C. Moon, J. Cusumano, and P. J. Holmes, Physica D **24**, 383 (1987).
[7] J.-C. Bacri, A. O. Cēbers, and R. Perzynski, Phys. Rev. Lett. **72**, 2705 (1994).
[8] A. Cēbers and S. Lācis, Brazilian J. Phys. **25**, 101 (1995).
[9] J.-C. Bacri, A. Cēbers, S. Lācis, and R. Perzynski, J. Magn. Magn. Mater. **149**, 143 (1995).
[10] J.-C. Bacri, A. Cēbers, S. Lācis, and R. Perzynski, Magnitnaja Gidrodinamika **31**, 49 (1995).
[11] S. Lācis, Magnitnaja Gidrodinamika **32**, 31 (1996).
[12] F. C. Moon, *Chaotic and Fractal Dynamics: an Introduction for Applied Scientists and Engineers* (Wiley Scientific, New York, 1992), p. 508.
[13] P. Bak, Phys. Today **39** (12), 38 (1986).
[14] E. Ott, *Chaos in Dynamical Systems* (Cambridge University Press, New York, 1993), p. 385.
[15] V. I. Arnold, *Geometrical Methods in the Theory of Ordinary Differential Equations* (Springer-Verlag, New York, 1983), p. 334.
[16] T. Bohr and G. Gunaratne, Phys. Lett. **113A**, 55 (1985).
[17] J. C. Bacri, A. Cēbers, S. Lācis, and R. Perzynski (unpublished).